JEM Journal of Experimental Medicine

ARTICLE

PDGF-D activation by macrophage-derived uPA promotes AngII-induced cardiac remodeling in obese mice

Yu-Wen Cheng[1*], Ze-Bei Zhang[1*], Bei-Di Lan[2], Jing-Rong Lin[1], Xiao-Hui Chen[1], Ling-Ran Kong[1], Lian Xu[1], Cheng-Chao Ruan[1], and Ping-Jin Gao[1]

Obesity-induced secretory disorder of adipose tissue–derived factors is important for cardiac damage. However, whether platelet-derived growth factor-D (PDGF-D), a newly identified adipokine, regulates cardiac remodeling in angiotensin II (AngII)–infused obese mice is unclear. Here, we found obesity induced PDGF-D expression in adipose tissue as well as more severe cardiac remodeling compared with control lean mice after AngII infusion. Adipocyte-specific PDGF-D knockout attenuated hypertensive cardiac remodeling in obese mice. Consistently, adipocyte-specific PDGF-D overexpression transgenic mice (PA-Tg) showed exacerbated cardiac remodeling after AngII infusion without high-fat diet treatment. Mechanistic studies indicated that AngII-stimulated macrophages produce urokinase plasminogen activator (uPA) that activates PDGF-D by splicing full-length PDGF-D into the active PDGF-DD. Moreover, bone marrow–specific uPA knockdown decreased active PDGF-DD levels in the heart and improved cardiac remodeling in HFD hypertensive mice. Together, our data provide for the first time a new interaction pattern between macrophage and adipocyte: that macrophage-derived uPA activates adipocyte-secreted PDGF-D, which finally accelerates AngII-induced cardiac remodeling in obese mice.

Introduction

Obesity and its metabolic complications fuel cardiovascular mortality and morbidity (Davis, 2017; Gibb and Hill, 2018; Kovell and Aurigemma, 2019; Lee et al., 2018). Many clinical and experimental investigations have established that obese adipose tissue enhances the risk of hypertension and related target organ damage, including cardiac remodeling, vascular dysfunction, and stroke (Chang et al., 2020; Lavie et al., 2017). Among these, hypertensive cardiac remodeling, characterized by compromised contractility, hypertrophy, and interstitial fibrosis, is the main cause of heart failure (Ambia et al., 2018; Porter and Turner, 2009; Ruan et al., 2018). Obesity-induced adipose tissue dysfunction leads to abnormal adipokine production, which plays a vital role in the regulation of cardiac remodeling (Martínez-Martínez et al., 2015; Packer, 2018). Our previous study showed that obesity induces platelet-derived growth factor-D (PDGF-D) expression in the adipocytes (Zhang et al., 2018). It is well known that the PDGF family, especially PDGF-B, plays a pivotal role in the regulation of cardiovascular homeostasis and disease (Andrae et al., 2008). However, little is known about the role of adipocyte-derived PDGF-D in the pathogenesis of obesity-related cardiovascular disease.

Chronic low-grade inflammation has been postulated to play an important role in the development of both obesity and hypertension (He et al., 2021; Mouton et al., 2020; Turer et al., 2012). This inflammatory response is characterized by excess macrophage activation and dysregulation of macrophage polarization (Sun et al., 2015). Recruited macrophages induce proinflammatory cytokine production that impairs adipose function during obesity as well as promotes cardiac remodeling in hypertension. However, little is known about the specific mechanism underlying the effect of macrophages in obesity combined with hypertension.

PDGF-D is secreted primarily in an inactive, full-length form and activated by urokinase plasminogen activator (uPA) or matriptase extracellularly (Folestad et al., 2018). The previous study showed that full-length PDGF-D promotes macrophage recruitment in the process of wound healing, indicating the possibility of PDGF-D activation in the presence of macrophage (Uutela et al., 2004). Therefore, we hypothesized that macrophage-derived factor(s) may be involved in the activation of adipocyte-secreted PDGF-D in obese mice.

[1]Department of Cardiovascular Medicine, State Key Laboratory of Medical Genomics, Shanghai Key Laboratory of Hypertension, Shanghai Institute of Hypertension, Ruijin Hospital, Shanghai Jiao Tong University School of Medicine, Shanghai, China; [2]Department of Cardiology, First Affiliated Hospital, Xi'an Jiao Tong University, Xi'an, Shanxi, China.

*Y.-W. Cheng and Z.-B. Zhang contributed equally to this paper; Correspondence to Cheng-Chao Ruan: ruancc@fudan.edu.cn; C.-C. Ruan's present address is Shanghai Key Laboratory of Bioactive Small Molecules, Department of Physiology and Pathophysiology, School of Basic Medical Sciences, Fudan University, Shanghai, China.

In the present study, we discovered abnormal induction of PDGF-D in adipose tissue of obese mice and determined the protective effects of adipocyte-specific PDGF-D KO (AT-PDGF-D KO) against pathological cardiac remodeling after angiotensin II (AngII) infusion. In addition, adipocyte-specific PDGF-D transgenic (PA-Tg) mice showed exacerbated cardiac remodeling after AngII infusion without high-fat diet (HFD) treatment. Macrophage depletion could block the effect of PA-Tg–accelerated cardiac remodeling in hypertension. Mechanically, we found that activated macrophages could produce uPA that splices full-length PDGF-D into an active form. Bone marrow–specific uPA knockdown improved cardiac remodeling in HFD hypertensive mice with a decreased active PDGF-D level. These findings suggest that the direct interaction between macrophage and adipocyte accelerates hypertensive cardiac remodeling during obesity.

Results

Obesity aggravates cardiac remodeling in hypertensive mice

We first determined cardiac pathological hypertrophy and fibrosis in mice fed 16 wk of HFD combined with AngII infusion during the last 4 wk or with low-fat diet (LFD) and saline infusion as control. HFD led to more severe cardiac dysfunction, reflected by a decreased ejection fraction (EF), fractional shortening (FS), and increased diastolic left ventricular internal dimension (LVID; D) and interventricular septum (IVS; D) detected by echocardiography compared with LFD mice after AngII infusion (Fig. 1, A and B). Wheat germ agglutinin (WGA), Sirius Red staining, and immunohistochemical (IHC) staining for collagen, type I, α 1 chain (Col1a1) were performed to analyze cardiac hypertrophy and interstitial fibrosis (Fig. 1 C). These histological analyses revealed that HFD increased cardiomyocyte size, fibrosis area, and Col1a1 expression compared with LFD mice after AngII infusion (Fig. 1 D). Consistently, HFD resulted in increased mRNA expression of fibrotic markers Col1a1, Col4a1, α-smooth muscle actin (αSMA), and hypertrophic markers, including atrial natriuretic polypeptide (ANP) and brain natriuretic peptide (BNP; Fig. 1 E).

Obesity-increased adipocyte-secreted PDGF-D accelerates AngII-induced cardiac remodeling

To determine whether PDGF-D is involved in the regulation of cardiac remodeling in obese mice, we assessed PDGF-D expression. As shown by quantitative PCR (qPCR), PDGF-D was abundantly expressed in adipose tissue, including interscapular brown adipose tissue (iBAT), subcutaneous adipose tissue (SAT), and perivascular adipose tissue (PVAT), while little was expressed in the heart, kidneys, and blood vessels (Fig. S1 A). More importantly, HFD further increased PDGF-D expression in adipose tissue, but not in several other tissues, whereas AngII had no significant effect on PDGF-D expression (Fig. 1 F and Fig. S1 B). The upregulation of PDGF-D in adipose tissue also caused an increase of PDGF-D in plasma of obese mice (Fig. 1 G). The increase of PDGF-D in adipose tissue was further confirmed by IHC staining and Western blot (Fig. 1 H and Fig. S1 C).

Next, we generated adipocyte-specific PDGF-D KO mice to demonstrate the specific role of adipocyte-derived PDGF-D in obesity-related hypertensive cardiac remodeling. PDGF-D$^{flox/+}$ mice were bred with Adipoq-Cre mice to produce the experimental mice, including Adipoq-Cre+; PDGF-D$^{flox/flox}$ (AT-PDGF-D KO) and littermates Adipoq-Cre–; PDGF-D$^{flox/flox}$ (control) mice (Fig. S2 A). These mice were subjected to HFD combined with AngII infusion as mentioned. AT-PDGF-D KO led to PDGF-D deficiency in adipose tissue but not in other tissues (Fig. S2 C). The lack of PDGF-D in adipose tissue is sufficient to cause the decrease of PDGF-D in plasma (Fig. S2 D). Although AT-PDGF-D KO did not affect blood pressure with AngII infusion or body weight in HFD induction (Fig. S2, E and F), echocardiography and histological analyses showed that AT-PDGF-D KO had increased EF and FS, decreased LVID; D and IVS; D (Fig. 2, A and B), and attenuated cardiomyocyte size, fibrotic area, and Col1a1 expression compared with control mice (Fig. 2, C and D). These pathological changes were accompanied by downregulating hypertrophic and fibrotic gene levels, including ANP, BNP, Col1a1, Col4a1, and αSMA, in AT-PDGF-D KO mice (Fig. 2 E).

To provide a more direct link between adipocyte-derived PDGF-D and hypertensive cardiac remodeling, we used PA-Tg mice (Fig. S2, G and H). Interestingly, adipocyte-specific PDGF-D overexpression aggravated AngII-induced cardiac remodeling in mice without HFD treatment (Fig. 3, A–E). These findings suggest that adipocyte-derived PDGF-D may be the direct cause for cardiac remodeling in obese mice with AngII infusion.

Macrophages are required for PDGF-D–aggravated hypertensive cardiac remodeling

To explore whether macrophages are involved in hypertensive cardiac remodeling under the obese state, we determined macrophage distribution in hearts of HFD mice. Immunofluorescence staining and flow cytometry assay suggested that macrophages were translocated to the heart by AngII but not HFD, indicating their involvement in hypertensive cardiac remodeling of PDGF-D–overexpressed mice (Fig. S3, A and B). The speculation was verified by the following in vitro experiment. The cardiac fibroblasts (CFs) were isolated from global PDGF-D KO mice to exclude cardiac resident PDGF-D interference. However, full-length PDGF-D induced CF proliferation and fibrotic protein expression only when co-cultured with bone marrow–derived macrophages (BMDMs; Fig. S3, C and D).

To determine the role of macrophages in PDGF-D–mediated cardiac remodeling in vivo, we depleted macrophages by using neutralizing antibody CSF-1R in PA-Tg mice (Fig. S3 E). Echocardiographic examination and histological analyses showed that macrophage depletion remarkably improved cardiac remodeling in PA-Tg mice with AngII infusion (Fig. S3, F–H). Taken together, these findings suggest that macrophages are required for adipocyte-derived PDGF-D–mediated hypertensive cardiac remodeling.

Macrophage-derived uPA activates adipocyte-secreted PDGF-D and promotes hypertensive cardiac remodeling

Full-length PDGF-D consists of CUB (complement C1r/C1s, Uegf, Bmp1) and growth factor domain. The CUB domain blocks the receptor-binding side and could be cleaved by uPA to form the active homodimer PDGF-DD (Fig. 4 A; Reigstad et al., 2005;

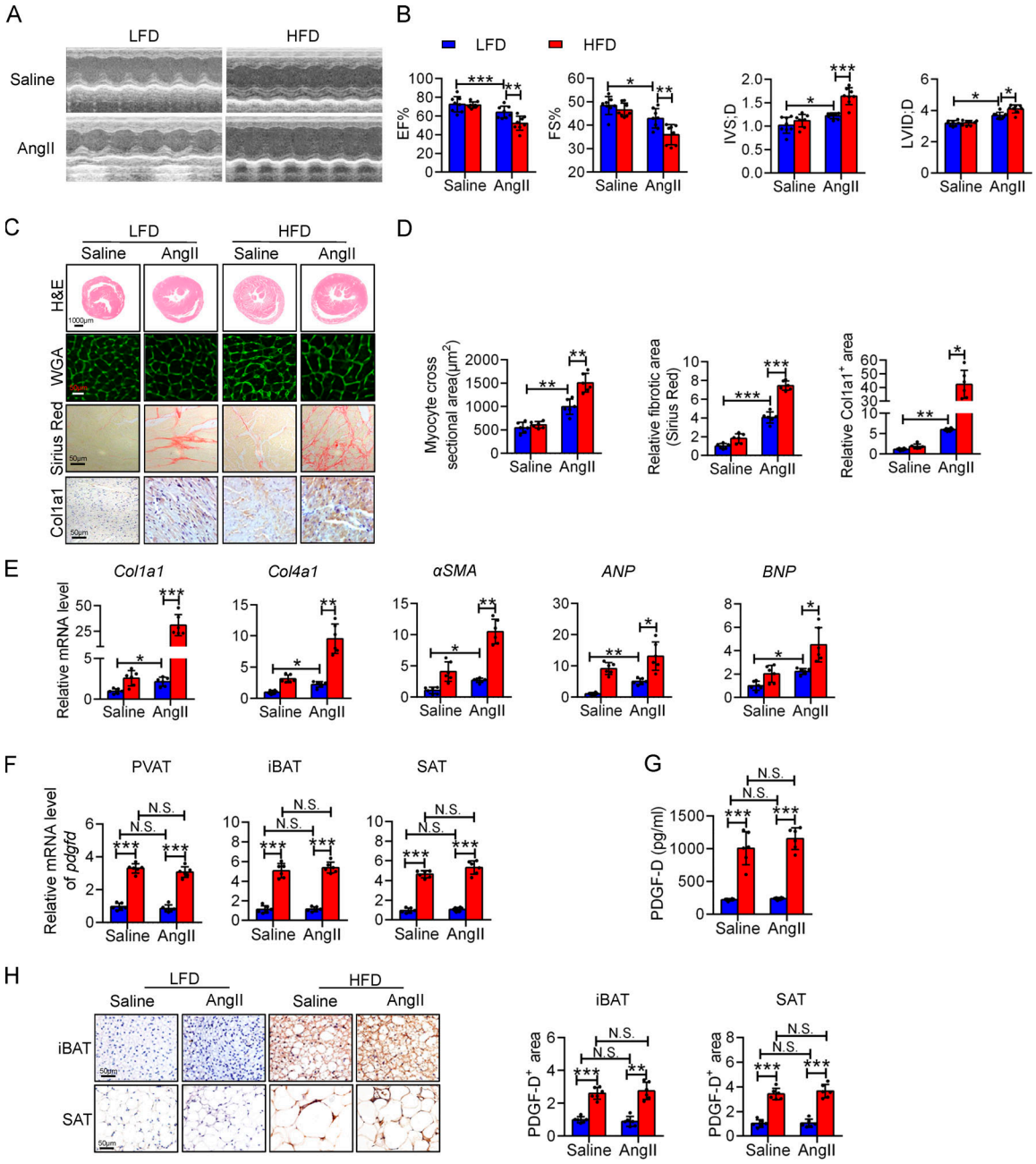

Figure 1. **HFD-induced obesity aggravates hypertensive cardiac remodeling and increases PDGF-D expression in adipose tissue. (A)** Representative echocardiography images of AngII-infused WT and HFD mice. **(B)** Quantitative analysis of EF, FS, LVID; D, and IVS; D obtained from echocardiography. *n* = 8. **(C)** Representative cross sections of hearts stained for H&E, Sirius Red, and WGA and IHC staining of Col1a1. Scale bar for WGA is 50 μm. **(D)** Quantitative analysis of cardiomyocyte size (WGA staining), fibrotic area (Sirius Red staining), and Col1a1 expression. *n* = 6. **(E)** qPCR analysis of hypertrophic (*ANP*; *BNP*) and fibrotic (*Col1a1*, *Col4a1*, and *αSMA*) genes in the heart. *n* = 6. **(F)** qPCR analysis of *pdgfd* gene in PVAT, iBAT, and SAT. *n* = 6. **(G)** PDGF-D level in plasma detected by ELISA. *n* = 6. **(H)** IHC staining and quantitative analysis of PDGF-D in iBAT and SAT. *n* = 6. All experimental data were verified in at least three independent experiments. Statistical significance was assessed using two-way ANOVA with Bonferroni post hoc test. Data are mean ± SD. *, P < 0.05; **, P < 0.01; ***, P < 0.001.

Ustach et al., 2010; Ustach and Kim, 2005). Interestingly, we found that cleaved PDGF-DD (30 kD), but not full-length PDGF-D (50 kD), increased in hearts of AngII-infused HFD mice and PA-Tg mice (Fig. 4 B and Fig. S4 A). Moreover, the phosphorylation of PDGFRβ (PDGF-DD receptor) was only increased in hearts of AngII-infused obese mice and PA-Tg mice (Fig. 4 B and Fig. S4 A). We next detected PDGF-D activator–uPA expression in different cells and tissues. The results exhibited that uPA was highly expressed in macrophages rather than in CFs and adipocytes (Fig. 4 C and Fig. S4 B). Double immunofluorescence staining showed that uPA was colocalized with F4/80-positive macrophages in hearts of AngII-infused mice (Fig. 4 D and Fig. S4 C). The expression of uPA was consistent with that of F4/80 all along, indicating that the increase of macrophage-derived

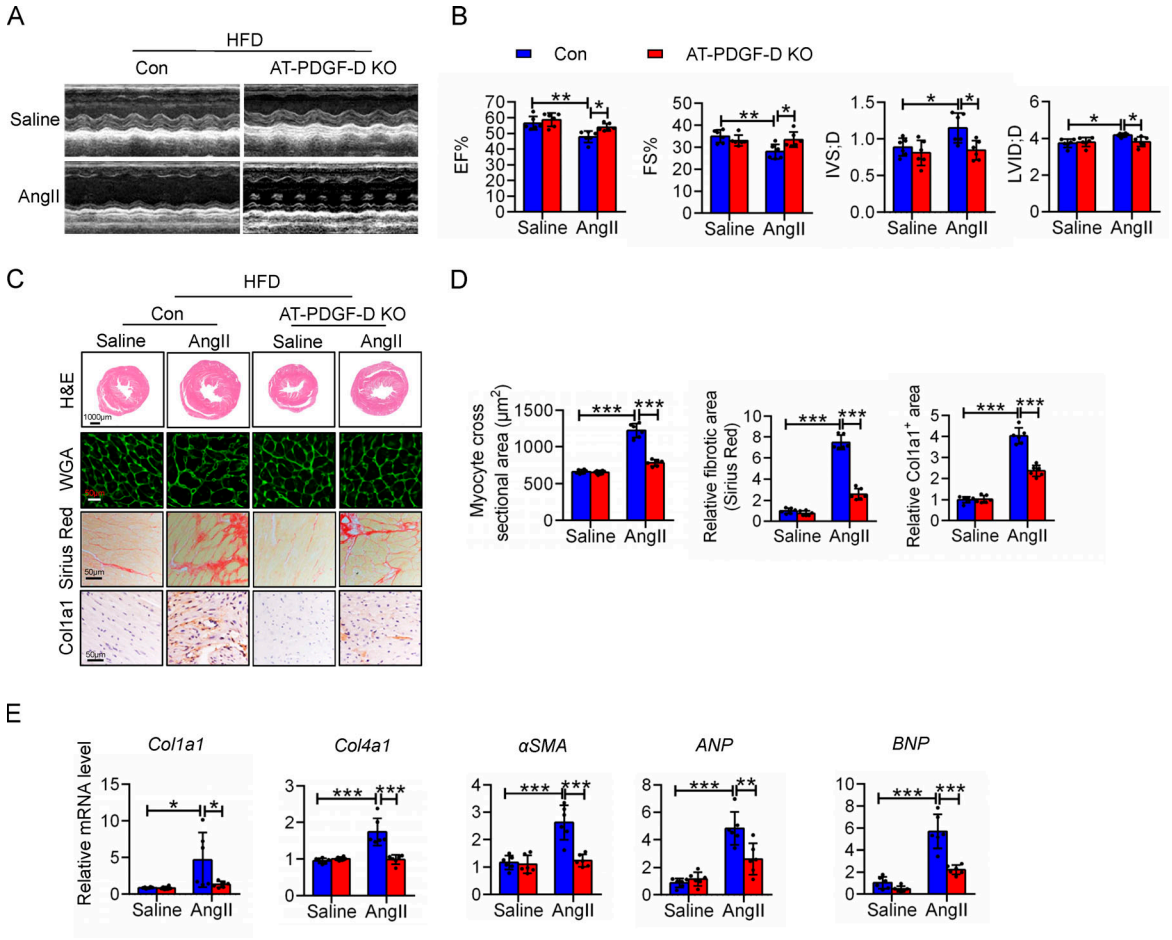

Figure 2. **Adipocyte-specific PDGF-D KO improves cardiac remodeling in obese mice. (A)** Representative echocardiography images of HFD-induced Adipoq-Cre−; PDGF-D$^{flox/flox}$ control (Con) and AT-PDGF-D KO obese mice infused with AngII. **(B)** Quantitative analysis of EF, FS, LVID; D, and IVS; D obtained from echocardiography. *n* = 6. **(C)** Representative cross sections of a heart stained for H&E, Sirius Red, and WGA and IHC staining of Col1a1. **(D)** Quantitative analysis of cardiomyocyte size (WGA staining), fibrotic area (Sirius Red staining), and Col1a1 expression. *n* = 6. **(E)** qPCR analysis of hypertrophic (*ANP* and *BNP*) and fibrotic (*Col1a1*, *Col4a1*, and *αSMA*) genes in the heart. *n* = 6. All experimental data were verified in at least two independent experiments. Statistical significance was assessed using two-way ANOVA with Bonferroni post hoc test. Data are mean ± SD. *, P < 0.05; **, P < 0.01; ***, P < 0.001.

uPA is mostly due to the increased quantity of macrophages by AngII induction. In addition, we found that only the combination of adipocyte conditional medium (AT-CM) from PA-Tg mice and macrophage conditional medium (M-CM) from WT mice could induce CF proliferation and fibrotic protein expression. Either absence of PDGF-D in AT-CM or knockdown of uPA in M-CM blocked these effects on CF function (Fig. 4, E and F). These findings suggest that PDGF-D was activated by macrophage-derived uPA in hearts of AngII-induced obese mice and PA-Tg mice.

To determine the role of macrophage-derived uPA in PDGF-D–mediated hypertensive cardiac remodeling in obese mice, we performed bone marrow transplantation (BMT) assays. Bone marrow cells of lean WT mice were infected with uPA shRNA lentivirus (BMT-sh-uPA) or control lentivirus (BMT-sh-Ctrl), and then injected into recipient HFD obese mice (Fig. 5, A–C). Two weeks after BMT, the mice were subjected to 4 wk AngII infusion. As the results showed, macrophage uPA had no effect on PDGF-D expression in heart or adipose tissue at the mRNA level (Fig. S4 D). However, BMT-sh-uPA attenuated the activated PDGF-DD level and PDGFRβ phosphorylation but not the full-length PDGF-D level in hearts of AngII-infused obese mice (Fig. 5 D). Besides, BMT-sh-uPA merely reduced the macrophage and uPA overlapped area but not the quantity of infiltrated macrophages in the heart (Fig. 5 E). More importantly, BMT-sh-uPA attenuated AngII-induced cardiac remodeling in HFD obese mice (Fig. 6, A–E). Consistently, AngII-induced cardiac remodeling was improved in BMT-sh-uPA PA-Tg mice (Fig. S5). These findings suggest that macrophage-secreted uPA is required for activating adipocyte-derived PDGF-D in regulating AngII-induced cardiac remodeling.

Active PDGF-DD promotes hypertensive cardiac remodeling through the PI3K-Akt signaling pathway

To determine the mechanism of how PDGF-DD contributes to hypertensive cardiac remodeling, we applied RNA sequencing in PDGF-DD–treated CFs. Primary CFs were also isolated from PDGF-D KO mice and stimulated by recombinant PDGF-DD for 12 h. As the results showed, differentially expressed genes were mostly distributed in terms of signal transduction (Fig. 7 A).

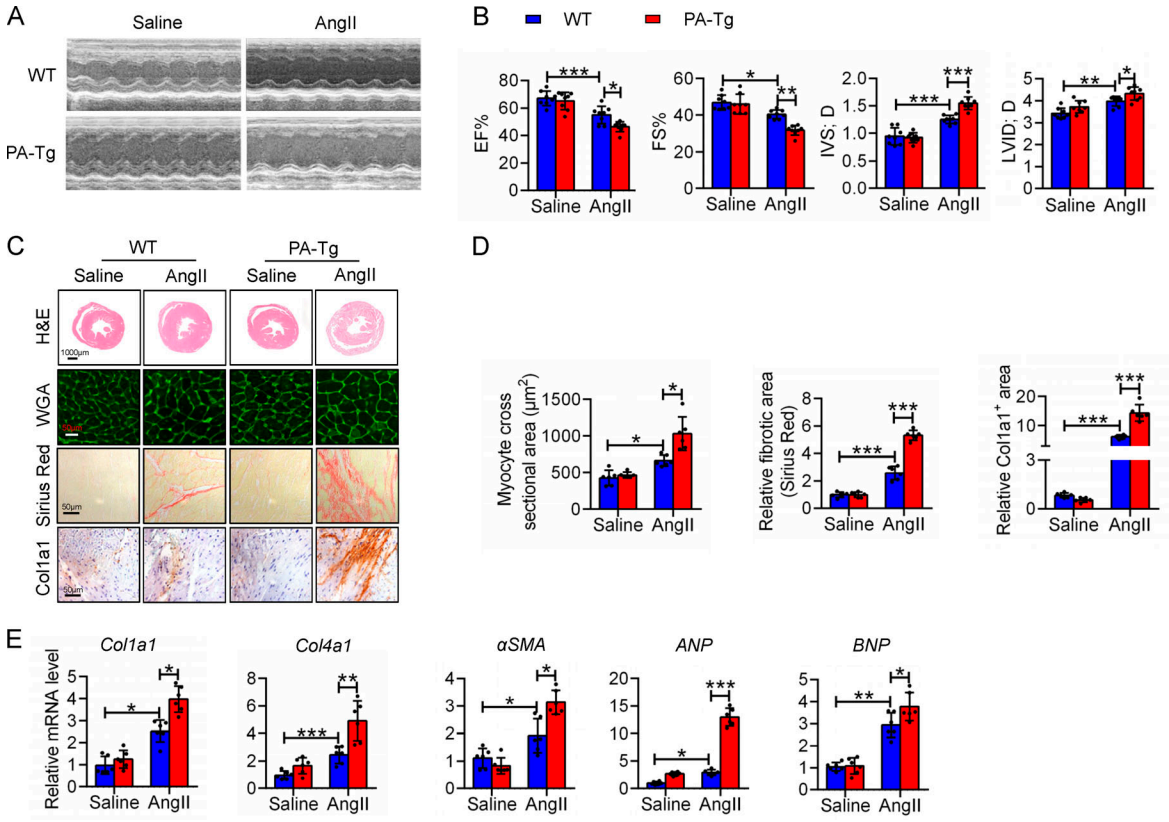

Figure 3. **Adipocyte-specific PDGF-D overexpression aggravates AngII-induced cardiac remodeling. (A)** Representative echocardiography images of WT and PA-Tg mice infused with saline or AngII. **(B)** Quantitative analysis of EF, FS, LVID; D, and IVS; D obtained from echocardiography. *n* = 8. **(C)** Representative cross sections of heart stained for H&E, Sirius Red, and WGA and IHC staining of Col1a1. **(D)** Quantitative analysis of cardiomyocyte size (WGA staining), fibrotic area (Sirius Red staining), and Col1a1 expression. *n* = 6. **(E)** qPCR analysis of hypertrophic (*ANP* and *BNP*) and fibrotic (*Col1a1*, *Col4a1*, and *αSMA*) genes in the heart. *n* = 6. All experimental data were verified in at least three independent experiments. Statistical significance was assessed using two-way ANOVA with Bonferroni post hoc test. Data are mean ± SD. *, P < 0.05; **, P < 0.01; ***, P < 0.001.

Kyoto Encyclopedia of Genes and Genomes (KEGG) analysis screened the most relevant pathway to our phenotype–PI3K-Akt signaling (Fig. 7 B). Gene set enrichment analysis of differentially expressed genes within PI3K-Akt signaling showed enrichment in fibrosis and hypertrophy (Fig. 7 C). These enriched categories confirmed the importance of the PI3K-Akt signaling pathway in PDGF-DD–promoted cardiac remodeling. Therefore, the activation of PI3K-Akt signaling pathway was measured in PDGF-DD–treated CFs, and perifosine was introduced to inhibit Akt phosphorylation, which is the core event of this pathway. Interestingly, PDGF-DD increased phosphorylation of PI3K and downstream Akt, CDK2, and P70S6K, which was attenuated by perifosine (Fig. 7 D). Consistently, perifosine restrained PDGF-DD–promoted proliferation, αSMA, and Col1a1 expression in CFs (Fig. 7, E and F). The enhanced activation of PI3K-Akt by PDGF-DD was verified in hearts of AngII-infused PA-Tg mice as well (Fig. 7 G). In conclusion, activated PDGF-DD contributed to cardiac remodeling via the PI3K-Akt signaling pathway (Fig. 7 H).

Discussion

In the present study, we uncovered a synergistic effect of adipocytes and macrophages in hypertensive cardiac remodeling during obesity. Several lines of direct evidence are provided to support our conclusion. First, by using adipocyte-specific PDGF-D KO or overexpression mice, we showed that adipocyte-derived PDGF-D was sufficient to aggravate or rescue cardiac remodeling in hypertensive obese mice, respectively. Second, macrophage-derived uPA is necessary for the effect of PDGF-D on CF activation. Finally, knockdown of macrophage uPA attenuates PDGF-D activation (forming PDGF-DD) and, hence, ameliorates hypertensive cardiac remodeling in obese or PA-Tg mice. In summary, adipocyte-secreted full-length PDGF-D is spliced by macrophage-derived uPA to form active PDGF-DD, which accelerates AngII-induced cardiac remodeling in HFD obese mice.

Resident PDGF-D has been suggested to induce cardiac fibrosis in heart-specific transgenic mice (Pontén et al., 2005), indicating the essential role of resident PDGF-D in cardiac remodeling. However, the previous study lacks PDGF-D expression data in adipose tissue, especially under the obese state. Adipose tissue is well known to function as a major endocrine organ that secretes adipokines, growth factors, cytokines, and chemokines (Longo et al., 2019; Oikonomou and Antoniades, 2019). Obesity-caused adipose tissue dysfunction results in an altered secretion pattern that contributes to the development of metabolic and cardiovascular diseases (Saxton et al., 2019).

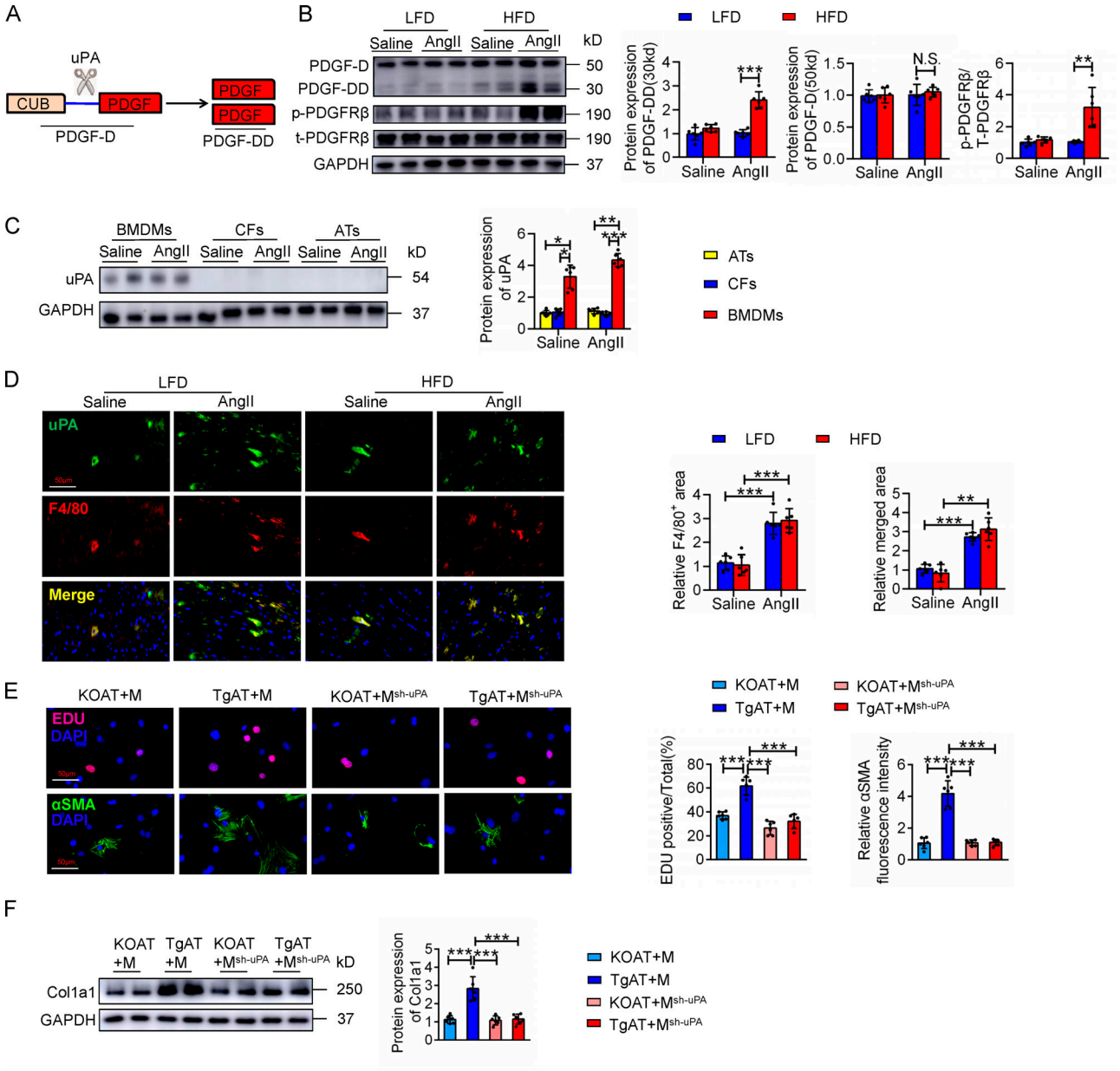

Figure 4. **Macrophage-derived uPA activates PDGF-D in hearts of AngII-induced obese mice. (A)** Diagram of PDGF-D structure and activation. **(B)** Western blot and quantitative analysis of full-length PDGF-D (50 kD), cleaved PDGF-DD (30 kD), phosphorylated-PDGFRβ (p-PDGFRβ), and total-PDGFRβ (t-PDGFRβ) expression in the heart. n = 6. **(C)** Western blot and quantitative analysis of uPA expression in BMDMs, CFs, and adipocytes (ATs). n = 6. **(D)** Representative images and quantitative analysis of double immunofluorescent staining of uPA and F4/80 in hearts of indicated mice. n = 6. **(E)** Representative images and quantitative analysis of EDU proliferation staining and immunofluorescent staining of αSMA in PDGF-D KO CFs. KOAT indicates AT-CM from PDGF-D KO mice; M indicates BMDM CM from WT mice; TgAT indicates AT CM from PA-Tg mice; $M^{sh\text{-}uPA}$ indicates CM of uPA knockdown BMDM. n = 6. **(F)** Western blot and quantitative analysis of Col1a1 expression in PDGF-D KO CFs. n = 6. All experimental data were verified in at least three independent experiments. Statistical significance was assessed using two-way ANOVA with Bonferroni post hoc test (B–D) or one-way ANOVA with Bonferroni post hoc test (E and F). Data are mean ± SD. *, P < 0.05; **, P < 0.01; ***, P < 0.001. Scale bars, 50 µm.

PDGF-D, a member of the PDGF family, is involved in the regulation of tissue fibrosis (Buhl et al., 2016; Klinkhammer et al., 2018; Kumar and Li, 2018). Herein, we indicated that PDGF-D primarily expresses in adipose tissue rather than in the heart, kidneys, and blood vessels. HFD-induced obesity promotes PDGF-D production and secretion from adipocytes. Blockade of PDGF-D or downstream signaling attenuates hypertensive cardiac remodeling in obese mice. It is worth noting that adipocyte-specific PDGF-D overexpression accelerates AngII-induced cardiac remodeling without HFD treatment. This suggests that abnormal PDGF-D production in adipocytes, but not obesity, contributes to hypertensive cardiac remodeling in obese mice.

PDGF-D is primarily secreted in a full-length form before proteolytic activation and functions as activated homodimer PDGF-DD (Fan et al., 2013; Lee and Li, 2018; Muhl et al., 2017; Ricci and Ferri, 2015). In addition to having the common

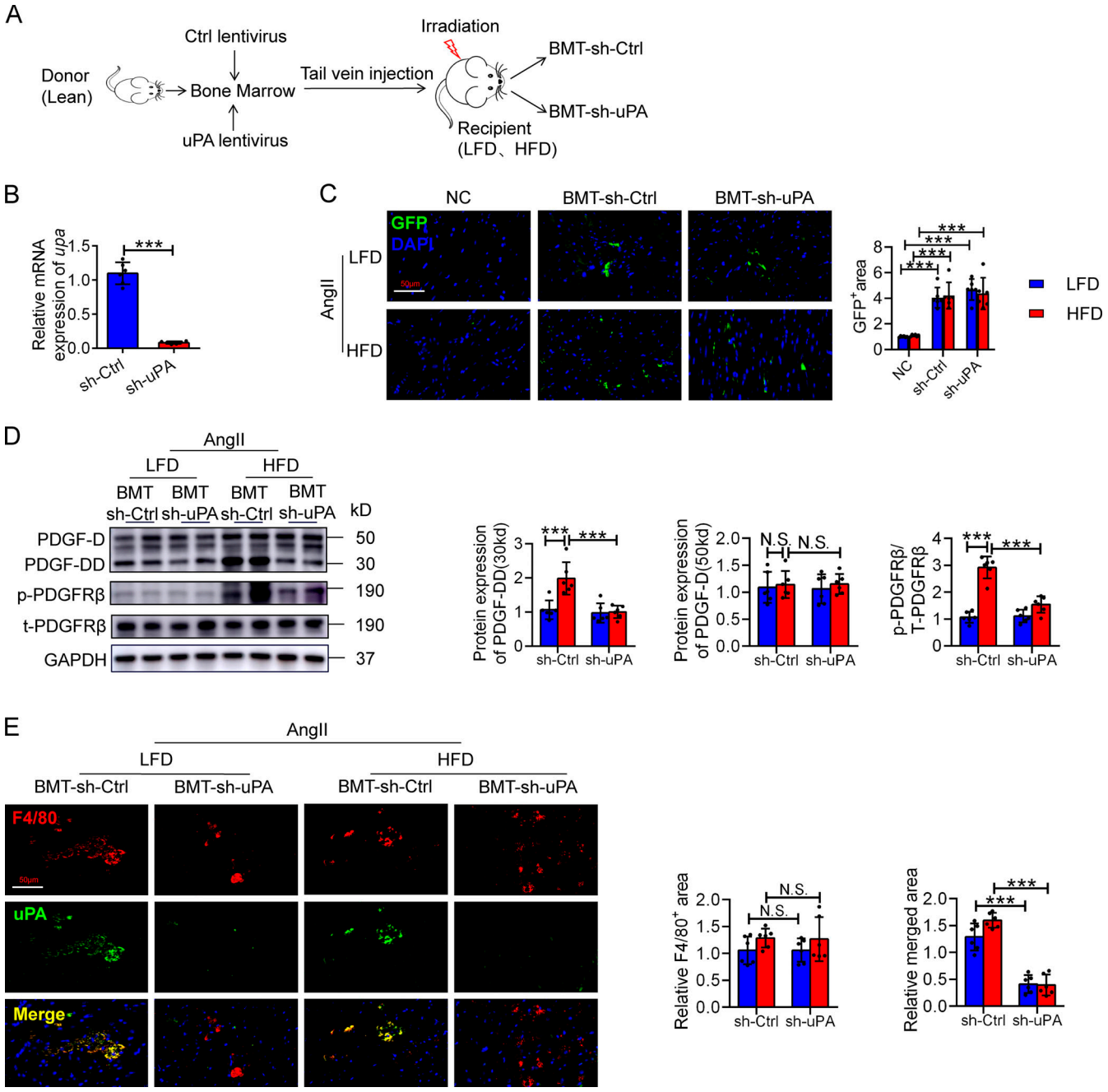

Figure 5. **Macrophage uPA knockdown decreases PDGF-D activation in obese mice. (A)** Illustration of BMT protocol. **(B)** The knockdown of uPA in lentivirus-infected BMDMs was verified by qPCR analysis. *n* = 6. **(C)** Representative images and quantitative analysis of immunofluorescent staining of GFP-positive macrophages in hearts of BMT-sh-Ctrl and BMT-sh-uPA mice. NC, negative control. *n* = 6. **(D)** Western blot and quantitative analysis of full-length PDGF-D (50 kD), cleaved PDGF-DD (30 kD), p-PDGFRβ, and t-PDGFRβ expression in hearts of LFD or HFD obese mice that received BMT-sh-Ctrl cells or BMT-sh-uPA cells with AngII infusion. *n* = 6. **(E)** Representative images and quantitative analysis of double immunofluorescent staining of uPA and F4/80 in hearts of indicated mice. *n* = 6. All experimental data were verified in at least two independent experiments. Statistical significance was assessed using an unpaired, two-tailed Student's *t* test (B) or two-way ANOVA with Bonferroni post hoc test (C–E). Data are mean ± SD. ***, P < 0.001. Scale bars, 50 µm.

structure of classic PDGFs, full-length PDGF-D has an additional unique N-terminal CUB domain (Andrae et al., 2008; Bergsten et al., 2001). The hinge region of PDGF-D between the CUB domain and the growth factor domain contains a cleavage site for proteolytic removal of the CUB domain, and then two growth factor domains form the active homodimer PDGF-DD (Bergsten et al., 2001; Reigstad et al., 2005). It has been reported that serine proteases uPA could splice full-length PDGF-D (Ehnman et al., 2009; Ustach et al., 2010; Ustach and Kim, 2005). The role of uPA in tissue remodeling is already well established. Previous data indicated that increased uPA contributes to organ fibrosis via promoting plasmin and ultimately the TGF-β pathway (Gupta et al., 2017; Smith and Marshall, 2010). However, the TGF-β pathway is not required for PDGF-DD–induced cardiac

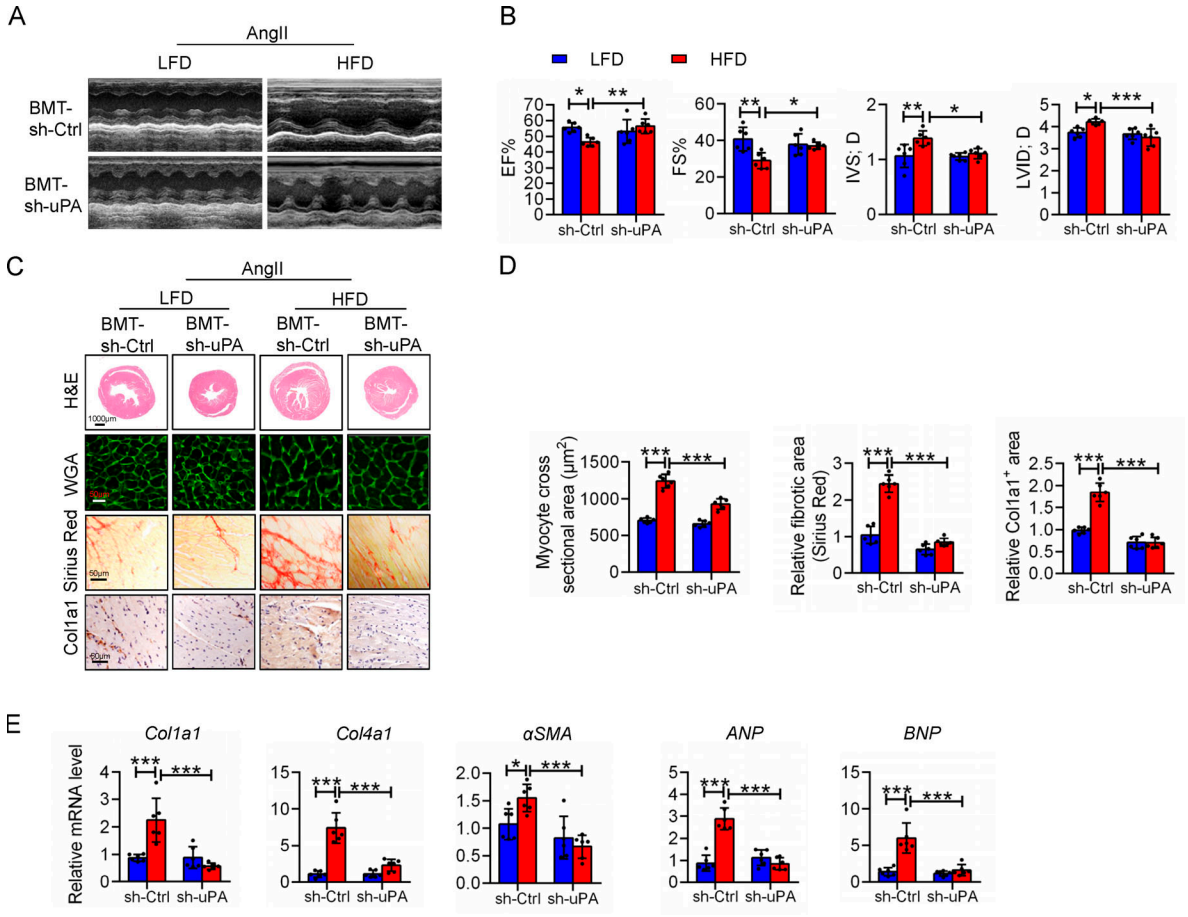

Figure 6. **Macrophage uPA knockdown ameliorates hypertensive cardiac remodeling of obese mice. (A)** Representative echocardiography images of LFD and HFD mice that received BMT-sh-Ctrl cells or BMT-sh-uPA cells with AngII infusion. **(B)** Quantitative analysis of EF, FS, LVID; D, and IVS; D obtained from echocardiography. *n* = 6. **(C)** Representative cross sections of heart stained for H&E, Sirius red, and WGA and IHC staining of Col1a1. **(D)** Quantitative analysis of cardiomyocyte size (WGA staining), fibrotic area (Sirius Red staining), and Col1a1 expression. *n* = 6. **(E)** qPCR analysis of hypertrophic (*ANP* and *BNP*) and fibrotic (*Col1a1*, *Col4a1*, and *αSMA*) genes in the heart. *n* = 6. All experimental data were verified in at least two independent experiments. Statistical significance was assessed using two-way ANOVA with Bonferroni post hoc test. Data are mean ± SD. *, P < 0.05; **, P < 0.01; ***, P < 0.001.

remodeling in the present obesity-related hypertensive model. Actually, PDGF-DD was proven to promote cardiac remodeling via PI3K-Akt signaling pathway. Besides, uPA stimulation stabilized p53 and induced human 8-oxoguanine DNA glycosylase, which protected cardiac myocytes from oxidative damage–induced apoptosis (Hohensinner et al., 2017). The damage effect in tissue remodeling and protective effect in apoptosis indicated a flexible cell type–specific property of uPA. Herein, we show that uPA is primarily expressed in the macrophages and detectable in hearts of AngII-infused mice because of increased macrophage infiltration. Hence, the encounter of macrophage-derived uPA by AngII-induction and adipocyte-derived PDGF-D by HFD treatment took place in the heart and contributed to cardiac remodeling synergistically. Over past decades, many studies demonstrated that adipocyte-secreted adipokines could regulate macrophage activation and subsequent inflammatory factor expression and then contribute to cardiovascular diseases. On the other hand, macrophage-derived inflammatory factors could also directly regulate adipocyte function and adipokine expression. However, to our knowledge, the present study provides the first experimental evidence that macrophage-derived factors activate adipocyte-secreted adipokines, which subsequently accelerate cardiac remodeling. The activation of adipocyte-derived PDGF-D by macrophage-derived uPA provides a new pattern of interaction between macrophages and adipocytes in obesity-related cardiovascular diseases.

In conclusion, this study demonstrates that activation of adipocyte-secreted PDGF-D by macrophage-derived uPA accelerates Ang II-induced cardiac remodeling in obese mice, which can be ameliorated via modulation of the uPA/PDGF-D pathway. Obesity and hypertension usually coexist in humans and are characterized by metabolic dysfunction and inflammation in the adipose tissue and heart. We provide a direct mechanism that obesity and hypertension synergistically promote cardiac injury. Notwithstanding the much more advanced complexity of human cardiac injury induced by obesity with hypertension in comparison with the mouse model, our novel findings suggest an attractive possibility that targeting the uPA/PDGF-D pathway might serve as a potential therapeutic tool for prevention of hypertensive cardiac injury during obesity.

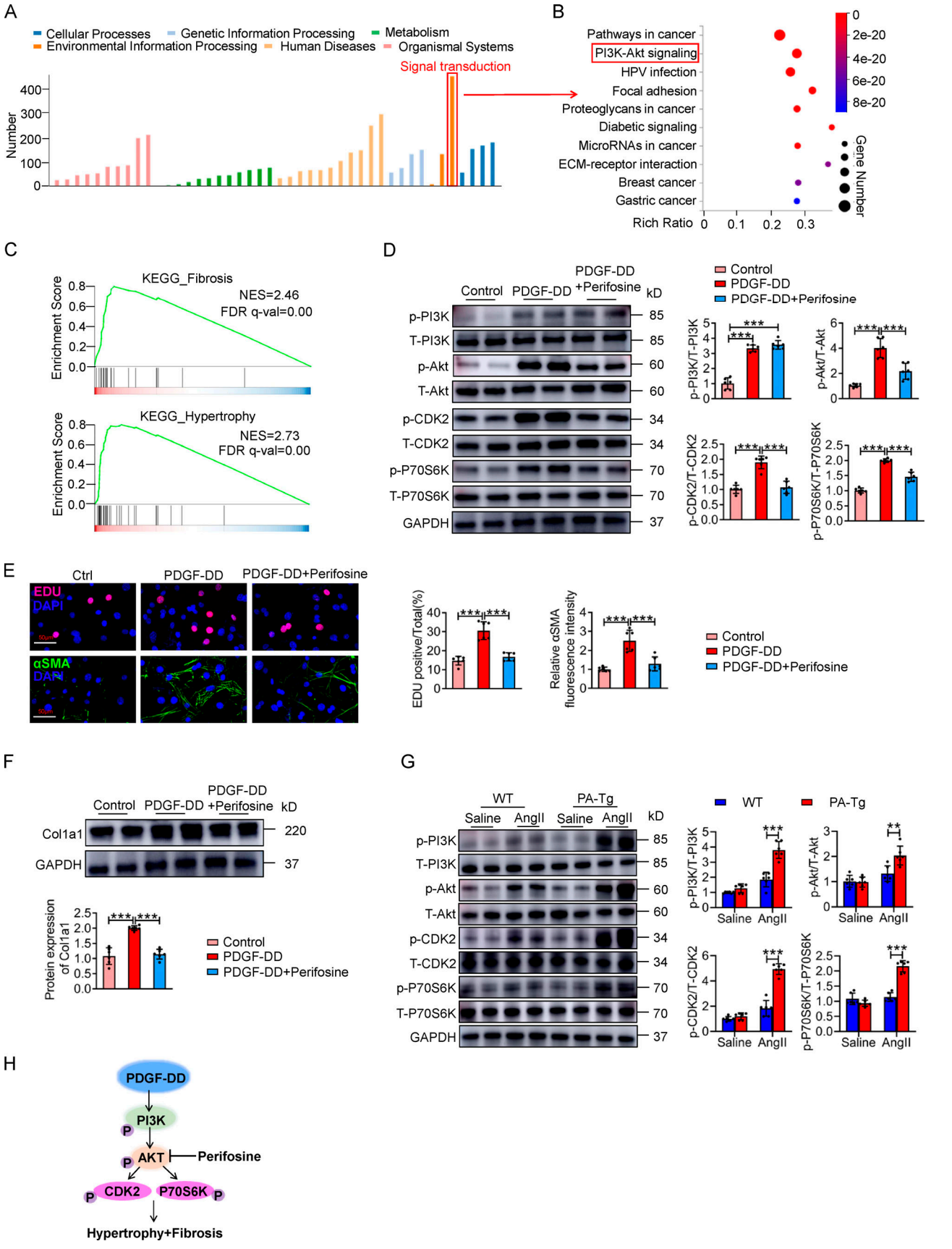

Figure 7. **PDGF-DD activates CFs via PI3K-Akt pathway. (A)** Primary PDGF-D KO CFs were cultured and stimulated by recombinant PDGF-DD (20 μM), and then total RNA was extracted and applied to RNA sequencing. Histogram of differentially expressed genes in control and PDGF-DD–treated CFs. **(B)** Bubble

chart of the top differentially expressed genes within KEGG categories of signal transduction. **(C)** GSEA of differentially expressed hypertrophy and fibrosis genes within the PI3K-Akt category. **(D)** Primary PDGF-D KO CFs were treated by recombinant PDGF-DD (20 µM) or Akt inhibitor perifosine (5 µM). Western blot and quantitative analysis of total-PI3K (T-PI3K), phosphorylated-PI3K (p-PI3K), total-Akt (T-Akt), phosphorylated-Akt (p-Akt), total-CDK2 (T-CDK2), phosphorylated-CDK2 (p-CDK2), total-P70S6K (T-P70S6K), and phosphorylated-P70S6K (p-P70S6K) in indicated CFs. $n = 6$. **(E)** Representative images and quantitative analysis of EDU proliferation staining and immunofluorescent staining of αSMA in CFs. $n = 6$. **(F)** Western blot and quantitative analysis of Col1a1 in CFs. GAPDH served as internal control, same with D, since the blots were performed in the same experiment. $n = 6$. **(G)** Western blot and quantitative analysis of T-PI3K, p-PI3K, T-Akt, p-Akt, T-CDK2, p-CDK2, T-P70S6K, and p-P70S6K in hearts of indicated mice. $n = 6$. **(H)** Diagram of the PDGF-DD-activated PI3K-Akt pathway. All experimental data were verified in at least three independent experiments. Statistical significance was assessed using one-way ANOVA with Bonferroni post hoc test (D–F) or two-way ANOVA with Bonferroni post hoc test (G). Data are mean ± SD. **, $P < 0.01$; ***, $P < 0.001$. Ctrl, control; ECM, extracellular matrix; FDR, false discovery rate; HPV, human papillomavirus; NES, normalized enrichment score. Scale bars, 50 µm.

Materials and methods

Animals and animal care

PDGF-D flox mice was generated by inserting flox sites on both sides of the *pdgf-d* exon via gene targeting method (Cyagen Biotechnology Co., Ltd.). PDGF-D flox mice were then bred with Adipoq-Cre mice (obtained from The Jackson Laboratory) to produce Adipoq-Cre+; PDGF-D flox heterozygote mice. The heterozygote mice were bred with PDGF-$D^{flox/flox}$ mice to produce AT-PDGF-D KO homozygote and littermate Adipoq-Cre–; PDGF-$D^{flox/flox}$ (control) mice (Fig. S2 A). Global PDGF-D KO mice were generated by interrupting PDGF-D exon by CRISPR/Cas9 (Cyagen Biotechnology; Fig. S2 B). PA-Tg mice were generated as previously described (Zhang et al., 2018). Briefly, a mouse *pdgf-d* open reading frame was inserted into the PiggyBac transposon gene expression vector after the adipocyte protein-2 promoter. Then, transgenic mice were generated by vector microinjection to the zygote (Fig. S2 G). PA-Tg mice were crossed with WT C57BL/6 mice, and nontransgenic littermates were used as control. HFD-induced obese mice were fed a diet containing 60% kcal from fat for 4 mo before and during the infusion of AngII. Mice in the normal diet group (LFD) were age matched to the HFD mice to control for the effects of aging. The mouse diets were purchased from Research Diets. The HFD (D12492) and LFD (D12450) have the same protein content (20% kcal), but the HFD contains 20% kcal from carbohydrates and 60% kcal from fat and the LFD contains 70% kcal from carbohydrates and 10% kcal from fat. Mice were infused with PBS or 1,000 ng/kg/min AngII using ALZET minipumps for 28 d. Systolic blood pressure was measured by the tail cuff method wherein conscious mice were restrained in a tube and tails attached to a Visitech detector (BP-2000). The average of three pressure readings was obtained. All animals had the same C57BL/6 background and free access to water and corresponding diet. All animal experiments were conducted in accordance with guidelines approved by the Institutional Guidelines established by the Committee of Ethics on Animal Experiments at Shanghai Jiao Tong University School of Medicine.

Echocardiography

Transthoracic echocardiography was performed with a Vevo 2100 instrument (Fuji Film Visual Sonics) equipped with an MS-400 imaging transducer (18–38 MHz). Mice were preconditioned by chest hair removal, anesthetized with 1%–2% isoflurane administered via inhalation, and maintained in a supine position on a dedicated animal handling platform with limbs attached for electrocardiogram gating during imaging. Body temperature was kept constant by feeding the signal of a rectal probe back to a heating pad while heart and respiratory rates were continuously monitored. M-mode recording was performed at the midventricular level. All images were obtained from parasternal LV long-axis view with heart rate maintained at 450–500 beats/min and analyzed using dedicated software (Vevo 2100 version 1.4). LV wall thickness (LVID; D) and IVS; D were measured. Percent LV EF and FS were calculated from M-mode measurements. All procedures were performed under double-blind conditions with regard to genotype or treatment.

Histological and immunostaining analysis

Heart and adipose tissues were fixed in 4% paraformaldehyde and embedded into paraffin, and then 5-mm sections were prepared for H&E and Sirius Red staining according to the manufacturer's instructions. For IHC staining, heart sections were incubated with primary antibody for Col1a1 (ab34710; Abcam), and adipose tissue sections were incubated with primary antibody for PDGF-D (40-2100; Invitrogen) and then HRP-conjugated secondary antibodies. For immunofluorescence staining, heart sections were incubated with primary antibodies for F4/80 (ab6640; Abcam) and uPA (17968-1-AP; Proteintech) and then fluorescence-conjugated secondary antibodies (Alexa Fluor 555, Alexa Fluor 488; Invitrogen). WGA staining was conducted using an FITC-conjugated probe (L4895; Sigma-Aldrich). Images of H&E, Sirius Red, and IHC staining were obtained by a Zeiss microscope. Immunofluorescence staining was examined by a laser-scanning confocal microscope (Zeiss). Images were analyzed with ImageJ and Image-Pro Plus software.

Real-time qPCR

Total RNA was extracted from tissues and cultured cells using TRIzol (Invitrogen) followed by chloroform extraction according to the manufacturer's protocol. RNA reverse transcription was performed using the PrimeScript RT Reagent Kit (Takara). Real-time qPCR was performed with an ABI PRISM 7900HT system (Applied Biosystems). Reactions were performed at 95°C for 30 s followed by 40 cycles at 95°C for 5 s, and at 60°C for 30 s. Relative expression of each gene was determined by normalizing to GAPDH. All primer sequences were listed in Table S1.

Western blot analysis

Mouse tissue or cell extracts containing equal amounts of total protein were resolved by SDS-PAGE followed by immunoblot with primary antibodies PDGF-D (Invitrogen, 40-2100), total-PDGFRβ (3169; Cell Signaling Technology), phosphorylated-PDGFRβ (3161;

Cell Signaling Technology), Col1a1 (91144S; Cell Signaling Technology), uPA (7968-1-AP; Proteintech), total-PI3K (4257T; Cell Signaling Technology), phosphorylated-PI3K (4228T; Cell Signaling Technology), total-Akt (9272; Cell Signaling Technology), phosphorylated-Akt (9271T; Cell Signaling Technology), total-CDK2 (2546T; Cell Signaling Technology), phosphorylated-CDK2 (2561S; Cell Signaling Technology), total-P70S6K (2708T; Cell Signaling Technology), phosphorylated-P70S6K (9234T; Cell Signaling Technology), and GAPDH (HRP-60004; Proteintech). The blots were probed with HRP-conjugated secondary antibodies, and the results of chemiluminescence were detected using an enhanced chemiluminescence detection system.

Cell culture

Primary preadipocytes were isolated from subcutaneous adipose tissue as previously described (Quesada-López et al., 2016). Briefly, subcutaneous adipose tissue of 5–6-wk-old mice were removed and digested by a collagenase method. Preadipocytes were then obtained by centrifugation. The preadipocytes were differentiated into adipocytes in 10% FBS DMEM/F12 culture medium supplemented with an adipogenic cocktail (0.5 mMIBMX, 1 mM dexamethasone, 1 mM rosiglitazone, 0.02 mM insulin, and 1 nM T3) for 48 h and then maintained in 0.02 mM insulin and 1 nM T3 and harvested at days 6–8 after differentiation. Primary CFs were isolated from 1–2-wk-old global PDGF-D KO mice as previously described (Dubey et al., 1998). Briefly, the heart was enzymatically digested and mechanically dissociated according to the manufacturer's instruction (130-098-373; Miltenyi Biotec). After dissociation, the sample was applied to a 70-µm filter to remove any remaining large particles from the CF suspension. CFs were cultured in DMEM supplemented with 15% FBS and 1% penicillin and streptomycin. CFs were treated with AngII (10×10^{-6} M), recombinant PDGF-DD (20 µM), perifosine (5 µM), or infected by recombinant lentiviruses. BMDMs were isolated and cultured as previously described (Hamers et al., 2012). In brief, bone marrow was flushed from long bones and washed with PBS and then suspended in DMEM supplemented with 10% L-cell CM. L-cell CM were collected from L929 cells cultured in T 75-cm^2 filter cap flasks in DMEM for 10 d and filtered through 0.2-µm filters. 7 d later, all nonadherent cells were removed and the remaining cells split into 12-well and 24-well plates.

Recombinant lentivirus

Mouse uPA shRNA and control scramble shRNA were constructed using GV493-GFP as follows: uPA shRNA sequence, 5′-CACTAC TATGGCTCTGAAA-3′, and no-target control shRNA sequence, 5′-TTCTCCGAACGTGTCACGT-3′. Full-length PDGF-D overexpression lentivirus was constructed using GV358-GFP. The sequence of full-length PDGF-D was obtained from NCBI. Lentiviruses were produced and purified by Shanghai GeneChem Co., Ltd. The viruses were used to infect cells in the presence of polybrene. The knockdown of uPA and overexpression of full-length PDGF-D were confirmed by qPCR.

Cell proliferation assay

CF proliferation assays were performed using Cell-Light EdU Apollo 594 In Vitro Imaging Kit (Ribobio Co., Ltd.). Briefly, we incubated live cells with 5-ethynyl-2′-deoxyuridine (EDU; 20 mM) for 1 h before fixation and stained nuclei according to the manufacturer's guidelines. Images were obtained by a laser scanning confocal microscope (Zeiss).

Immunocytochemistry

CFs were fixed in methanol, blocked with 1% BSA, and incubated with primary antibodies to αSMA (A5228, 1:100; Sigma-Aldrich). Immunofluorescent staining was completed by incubating the cells with secondary antibodies (Alexa Fluor 488, A21206 1:200; Invitrogen). Cellular nuclei were stained with DAPI (D1306, 1:1,000; Invitrogen). Images were obtained by a laser scanning confocal microscope (Zeiss).

Depletion of macrophages

In vivo macrophage depletion was conducted by neutralizing antibody CSF-1R. The anti–CSF-1R antibody was purchased from Bioxcell (BP0213). Mice were injected intraperitoneally with anti–CSF-1R (1 mg) every 2 d during AngII infusion.

Flow cytometry analysis

To determine macrophage translocation to the heart by AngII induction, heart samples were collected and digested to single-cell suspensions by collagenase I (2 mg/ml) and collagenase XI (0.15 mg/ml). Heart samples were subjected to Percoll (17089102; GE) gradient centrifugation before flow cytometric staining. Samples were analyzed using a Gallios Flow Cytometer (Beckman Coulter) and analyzed by FlowJo (version 10) software. The following antibodies were used: CD45-FITC (11-0451-85; eBioscience) and F4/80-eFluor 450 (48-4801-82; eBioscience).

BMT

BMT analyses were performed as previously described (Hamers et al., 2012). Briefly, donor bone marrow was isolated from 5–6-wk-old WT mice. Then, donor bone marrow was infected by uPA or sham lentivirus before transplantation. Recipient mice (PA-Tg or obese mice) were subjected to 10-Gy lethal-dose irradiation and received 1×10^7 bone marrow cells from donor mice 4 h later. After 2 wk, the infusion of AngII started. The recipient mice were fed with autoclaved water (pH 2.6) 1 wk before the BMT and lasted until the end of the hypertensive model.

RNA sequencing and analysis

Total RNA was extracted by TRIzol reagent according to the manufacturer's instructions. The quality of RNA was examined by a 2100 Bioanalyzer (Agilent), and the quantitation was examined by NanoDrop 2000. The RNA samples with RNA Integrity Number ≥8 were selected for preparing libraries. The RNA sequencing libraries were performed using TruSeq RNA Library Prep Kit v2 (Illumina). Paired-end sequencing (2 × 150 bp) of the libraries was performed in HiSeq 2500 (Illumina). The data mining and figure presentation process, including the gene ontology term analysis, KEGG, and GSEA, were all done by the BGI in-house customized data mining system called Dr.Tom, which combined different published software. The accession no. in the Gene Expression Omnibus is GSE175572.

Statistical analysis

The sample size (n = 6–8) of each experiment was estimated by power calculations based on data from previous studies and preliminary experiments. According to Power Analysis and Sample Size 2020 software, the power with respect to an α level of 0.05 is 0.93 (n = 6) or 0.98 (n = 8). Results are presented as mean ± SD and analyzed using GraphPad Prism 8.4 (GraphPad Software). All datasets ($n \geq 6$) were subjected to the Shapiro-Wilk test for the normality distribution analysis. Normally distributed data were analyzed using the unpaired, two-tailed Student's t test (for comparing two groups), one-way ANOVA (one independent variable), or two-way ANOVA (two independent variables) with Bonferroni post hoc test (for multigroup comparisons). For the datasets that did not follow a normal distribution, a nonparametric test, such as the Kruskal-Wallis test (for multigroup comparisons) or two-tailed Mann-Whitney test (for comparing two groups), was used. $P < 0.05$ was considered statistically significant.

Online supplemental material

Fig. S1 shows PDGF-D expression in control LFD and HFD mice. Fig. S2 shows AT-PDGF-D KO and PA-Tg mouse construction. Fig. S3 shows that macrophages are required in the PDGF-D–aggravated cardiac remodeling in vitro and in vivo. Fig. S4 shows that macrophage-derived uPA has no effect on PDGF-D expression but activates PDGF-D in hearts of AngII-induced PA-Tg mice. Fig. S5 shows that macrophage uPA knockdown ameliorates cardiac remodeling of PA-Tg mice. Table S1 lists primers for qPCR.

Acknowledgments

We sincerely thank Dr. Chen Yan (Aab Cardiovascular Research Institute, University of Rochester School of Medicine and Dentistry) for her valuable suggestions and critical reading of the article.

This work was support by grants from the National Natural Science Foundation of China (8203006, 81900218, 81922004, 81800225, 81870180), Shanghai Science and Technology Commission (19JC1414600), Shanghai Municipal Commission of Health and Family Planning (20184Y0140), and Shanghai Municipal Education Commission (18CG15).

Author contributions: P.-J. Gao, C.-C. Ruan, Z.-B. Zhang, and Y.-W. Cheng designed the experiments and wrote the paper. Y.-W. Cheng and Z.-B. Zhang performed the animal experiments and analytical methods. Y.-W. Cheng, Z.-B. Zhang, and B.-D. Lan performed the in vivo images. J.-R. Lin, X.-H. Chen, L.-R. Kong, and L. Xu performed in vitro work on adipocytes, cardiac myocytes, and fibroblasts. C.-C. Ruan and P.-J. Gao analyzed the data.

Disclosures: The authors declare no competing interests exist.

Submitted: 31 January 2021
Revised: 3 May 2021
Accepted: 9 June 2021

References

Ambia, A.M., J.L. Morgan, C.E. Wells, S.W. Roberts, M. Sanghavi, D.B. Nelson, and F.G. Cunningham. 2018. Perinatal outcomes associated with abnormal cardiac remodeling in women with treated chronic hypertension. *Am. J. Obstet. Gynecol.* 218:519.e1–519.e7. https://doi.org/10.1016/j.ajog.2018.02.015

Andrae, J., R. Gallini, and C. Betsholtz. 2008. Role of platelet-derived growth factors in physiology and medicine. *Genes Dev.* 22:1276–1312. https://doi.org/10.1101/gad.1653708

Bergsten, E., M. Uutela, X. Li, K. Pietras, A. Östman, C.-H. Heldin, K. Alitalo, and U. Eriksson. 2001. PDGF-D is a specific, protease-activated ligand for the PDGF beta-receptor. *Nat. Cell Biol.* 3:512–516. https://doi.org/10.1038/35074588

Buhl, E.M., S. Djudjaj, J. Babickova, B.M. Klinkhammer, E. Folestad, E. Borkham-Kamphorst, R. Weiskirchen, K. Hudkins, C.E. Alpers, U. Eriksson, et al. 2016. The role of PDGF-D in healthy and fibrotic kidneys. *Kidney Int.* 89:848–861. https://doi.org/10.1016/j.kint.2015.12.037

Chang, L., M.T. Garcia-Barrio, and Y.E. Chen. 2020. Perivascular adipose tissue regulates vascular function by targeting vascular smooth muscle cells. *Arterioscler. Thromb. Vasc. Biol.* 40:1094–1109. https://doi.org/10.1161/ATVBAHA.120.312464

Davis, J. 2017. Putting the brakes on hypertensive remodeling: an ATF3 mechanism of myofibroblast restraint. *Circulation.* 135:2058–2061. https://doi.org/10.1161/CIRCULATIONAHA.117.028020

Dubey, R.K., D.G. Gillespie, and E.K. Jackson. 1998. Adenosine inhibits collagen and protein synthesis in cardiac fibroblasts: role of A2B receptors. *Hypertension.* 31:943–948. https://doi.org/10.1161/01.HYP.31.4.943

Ehnman, M., H. Li, L. Fredriksson, K. Pietras, and U. Eriksson. 2009. The uPA/uPAR system regulates the bioavailability of PDGF-DD: implications for tumour growth. *Oncogene.* 28:534–544. https://doi.org/10.1038/onc.2008.410

Fan, B., L. Ma, Q. Li, L. Wang, J. Zhou, and J. Wu. 2013. Correlation between platelet-derived growth factor signaling pathway and inflammation in desoxycorticosterone-induced salt-sensitive hypertensive rats with myocardial fibrosis. *Int. J. Clin. Exp. Pathol.* 6:2468–2475.

Folestad, E., A. Kunath, and D. Wågsäter. 2018. PDGF-C and PDGF-D signaling in vascular diseases and animal models. *Mol. Aspects Med.* 62:1–11. https://doi.org/10.1016/j.mam.2018.01.005

Gibb, A.A., and B.G. Hill. 2018. Metabolic coordination of physiological and pathological cardiac remodeling. *Circ. Res.* 123:107–128. https://doi.org/10.1161/CIRCRESAHA.118.312017

Gupta, K.K., D.L. Donahue, M.J. Sandoval-Cooper, F.J. Castellino, and V.A. Ploplis. 2017. Plasminogen activator inhibitor-1 protects mice against cardiac fibrosis by inhibiting urokinase-type plasminogen activator-mediated plasminogen activation. *Sci. Rep.* 7:365. https://doi.org/10.1038/s41598-017-00418-y

Hamers, A.A., M. Vos, F. Rassam, G. Marinković, K. Kurakula, P.J. van Gorp, M.P. de Winther, M.J. Gijbels, V. de Waard, and C.J. de Vries. 2012. Bone marrow-specific deficiency of nuclear receptor Nur77 enhances atherosclerosis. *Circ. Res.* 110:428–438. https://doi.org/10.1161/CIRCRESAHA.111.260760

He, F., Y. Huang, Z. Song, H.J. Zhou, H. Zhang, R.J. Perry, G.I. Shulman, and W. Min. 2021. Mitophagy-mediated adipose inflammation contributes to type 2 diabetes with hepatic insulin resistance. *J. Exp. Med.* 218:e20201416. https://doi.org/10.1084/jem.20201416

Hohensinner, P.J., N. Takacs, C. Kaun, B. Thaler, K.A. Krychtiuk, S. Pfaffenberger, A. Aliabadi, A. Zuckermann, K. Huber, and J. Wojta. 2017. Urokinase plasminogen activator protects cardiac myocytes from oxidative damage and apoptosis via hOGG1 induction. *Apoptosis.* 22:1048–1055. https://doi.org/10.1007/s10495-017-1388-9

Klinkhammer, B.M., J. Floege, and P. Boor. 2018. PDGF in organ fibrosis. *Mol. Aspects Med.* 62:44–62. https://doi.org/10.1016/j.mam.2017.11.008

Kovell, L.C., and G.P. Aurigemma. 2019. Progressive adverse cardiac remodeling and obesity: unwelcome news from "the city that never sleeps". *J. Am. Soc. Echocardiogr.* 32:1326–1330. https://doi.org/10.1016/j.echo.2019.08.006

Kumar, A., and X. Li. 2018. PDGF-C and PDGF-D in ocular diseases. *Mol. Aspects Med.* 62:33–43. https://doi.org/10.1016/j.mam.2017.10.002

Lavie, C.J., A. Pandey, D.H. Lau, M.A. Alpert, and P. Sanders. 2017. Obesity and atrial fibrillation prevalence, pathogenesis, and prognosis: effects of weight loss and exercise. *J. Am. Coll. Cardiol.* 70:2022–2035. https://doi.org/10.1016/j.jacc.2017.09.002

Lee, C., and X. Li. 2018. Platelet-derived growth factor-C and -D in the cardiovascular system and diseases. *Mol. Aspects Med.* 62:12–21. https://doi.org/10.1016/j.mam.2017.09.005

Lee, J.M., V. Govindarajah, B. Goddard, A. Hinge, D.E. Muench, M.D. Filippi, B. Aronow, J.A. Cancelas, N. Salomonis, H.L. Grimes, and D. Reynaud. 2018. Obesity alters the long-term fitness of the hematopoietic stem cell compartment through modulation of *Gfi1* expression. *J. Exp. Med.* 215: 627–644. https://doi.org/10.1084/jem.20170690

Longo, M., F. Zatterale, J. Naderi, L. Parrillo, P. Formisano, G.A. Raciti, F. Beguinot, and C. Miele. 2019. Adipose tissue dysfunction as determinant of obesity-associated metabolic complications. *Int. J. Mol. Sci.* 20: 2358. https://doi.org/10.3390/ijms20092358

Martínez-Martínez, E., N. López-Ándres, R. Jurado-López, E. Rousseau, M.V. Bartolomé, A. Fernández-Celis, P. Rossignol, F. Islas, A. Antequera, S. Prieto, et al. 2015. Galectin-3 participates in cardiovascular remodeling associated with obesity. *Hypertension.* 66:961–969. https://doi.org/10.1161/HYPERTENSIONAHA.115.06032

Mouton, A.J., X. Li, M.E. Hall, and J.E. Hall. 2020. Obesity, hypertension, and cardiac dysfunction: novel roles of immunometabolism in macrophage activation and inflammation. *Circ. Res.* 126:789–806. https://doi.org/10.1161/CIRCRESAHA.119.312321

Muhl, L., E.B. Folestad, H. Gladh, Y. Wang, C. Moessinger, L. Jakobsson, and U. Eriksson. 2017. Neuropilin 1 binds PDGF-D and is a co-receptor in PDGF-D-PDGFRβ signaling. *J. Cell Sci.* 130:1365–1378. https://doi.org/10.1242/jcs.200493

Oikonomou, E.K., and C. Antoniades. 2019. The role of adipose tissue in cardiovascular health and disease. *Nat. Rev. Cardiol.* 16:83–99. https://doi.org/10.1038/s41569-018-0097-6

Packer, M. 2018. Epicardial adipose tissue may mediate deleterious effects of obesity and inflammation on the myocardium. *J. Am. Coll. Cardiol.* 71: 2360–2372. https://doi.org/10.1016/j.jacc.2018.03.509

Pontén, A., E.B. Folestad, K. Pietras, and U. Eriksson. 2005. Platelet-derived growth factor D induces cardiac fibrosis and proliferation of vascular smooth muscle cells in heart-specific transgenic mice. *Circ. Res.* 97: 1036–1045. https://doi.org/10.1161/01.RES.0000190590.31545.d4

Porter, K.E., and N.A. Turner. 2009. Cardiac fibroblasts: at the heart of myocardial remodeling. *Pharmacol. Ther.* 123:255–278. https://doi.org/10.1016/j.pharmthera.2009.05.002

Quesada-López, T., R. Cereijo, J.V. Turatsinze, A. Planavila, M. Cairó, A. Gavaldà-Navarro, M. Peyrou, R. Moure, R. Iglesias, M. Giralt, et al. 2016. The lipid sensor GPR120 promotes brown fat activation and FGF21 release from adipocytes. *Nat. Commun.* 7:13479. https://doi.org/10.1038/ncomms13479

Reigstad, L.J., J.E. Varhaug, and J.R. Lillehaug. 2005. Structural and functional specificities of PDGF-C and PDGF-D, the novel members of the platelet-derived growth factors family. *FEBS J.* 272:5723–5741. https://doi.org/10.1111/j.1742-4658.2005.04989.x

Ricci, C., and N. Ferri. 2015. Naturally occurring PDGF receptor inhibitors with potential anti-atherosclerotic properties. *Vascul. Pharmacol.* 70:1–7. https://doi.org/10.1016/j.vph.2015.02.002

Ruan, C.C., L.R. Kong, X.H. Chen, Y. Ma, X.X. Pan, Z.B. Zhang, and P.J. Gao. 2018. A_{2A} receptor activation attenuates hypertensive cardiac remodeling via promoting brown adipose tissue-derived FGF21. *Cell Metab.* 28: 476–489.e5. https://doi.org/10.1016/j.cmet.2018.06.013

Saxton, S.N., B.J. Clark, S.B. Withers, E.C. Eringa, and A.M. Heagerty. 2019. Mechanistic links between obesity, diabetes, and blood pressure: role of perivascular adipose tissue. *Physiol. Rev.* 99:1701–1763. https://doi.org/10.1152/physrev.00034.2018

Smith, H.W., and C.J. Marshall. 2010. Regulation of cell signalling by uPAR. *Nat. Rev. Mol. Cell Biol.* 11:23–36. https://doi.org/10.1038/nrm2821

Sun, W., Y. Pang, Z. Liu, L. Sun, B. Liu, M. Xu, Y. Dong, J. Feng, C. Jiang, W. Kong, and X. Wang. 2015. Macrophage inflammasome mediates hyperhomocysteinemia-aggravated abdominal aortic aneurysm. *J. Mol. Cell. Cardiol.* 81:96–106. https://doi.org/10.1016/j.yjmcc.2015.02.005

Turer, A.T., J.A. Hill, J.K. Elmquist, and P.E. Scherer. 2012. Adipose tissue biology and cardiomyopathy: translational implications. *Circ. Res.* 111: 1565–1577. https://doi.org/10.1161/CIRCRESAHA.111.262493

Ustach, C.V., and H.R. Kim. 2005. Platelet-derived growth factor D is activated by urokinase plasminogen activator in prostate carcinoma cells. *Mol. Cell. Biol.* 25:6279–6288. https://doi.org/10.1128/MCB.25.14.6279-6288.2005

Ustach, C.V., W. Huang, M.K. Conley-LaComb, C.Y. Lin, M. Che, J. Abrams, and H.R. Kim. 2010. A novel signaling axis of matriptase/PDGF-D/ß-PDGFR in human prostate cancer. *Cancer Res.* 70:9631–9640. https://doi.org/10.1158/0008-5472.CAN-10-0511

Uutela, M., M. Wirzenius, K. Paavonen, I. Rajantie, Y. He, T. Karpanen, M. Lohela, H. Wiig, P. Salven, K. Pajusola, et al. 2004. PDGF-D induces macrophage recruitment, increased interstitial pressure, and blood vessel maturation during angiogenesis. *Blood.* 104:3198–3204. https://doi.org/10.1182/blood-2004-04-1485

Zhang, Z.B., C.C. Ruan, J.R. Lin, L. Xu, X.H. Chen, Y.N. Du, M.X. Fu, L.R. Kong, D.L. Zhu, and P.J. Gao. 2018. Perivascular adipose tissue-derived PDGF-D contributes to aortic aneurysm formation during obesity. *Diabetes.* 67: 1549–1560. https://doi.org/10.2337/db18-0098

Supplemental material

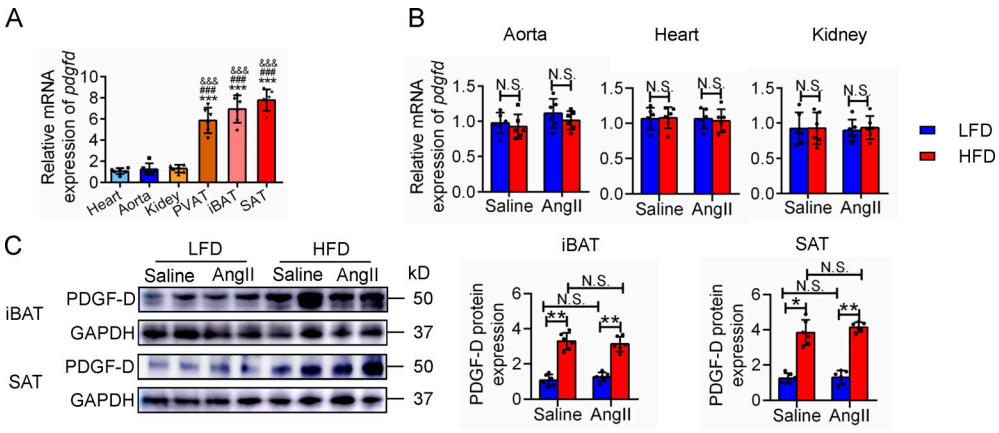

Figure S1. **PDGF-D expression in control LFD and HFD mice. (A)** qPCR analysis of *pdgfd* in heart, aorta, kidney, PVAT, iBAT, and SAT of WT mice. *n* = 6. **(B)** qPCR analysis of *pdgfd* in heart, aorta, and kidney of LFD and HFD mice. *n* = 6. **(C)** Western blot and quantitative analysis of PDGF-D expression in iBAT and SAT. *n* = 6. All experimental data were verified in at least two independent experiments. Statistical significance was assessed using one-way ANOVA with Bonferroni post hoc test (A) or two-way ANOVA with Bonferroni post hoc test (B and C). Data are mean ± SD. *, P < 0.05; **, P < 0.01; ***, P < 0.001 versus heart. ###, P < 0.001 versus aorta. &&&, P < 0.001 versus kidney.

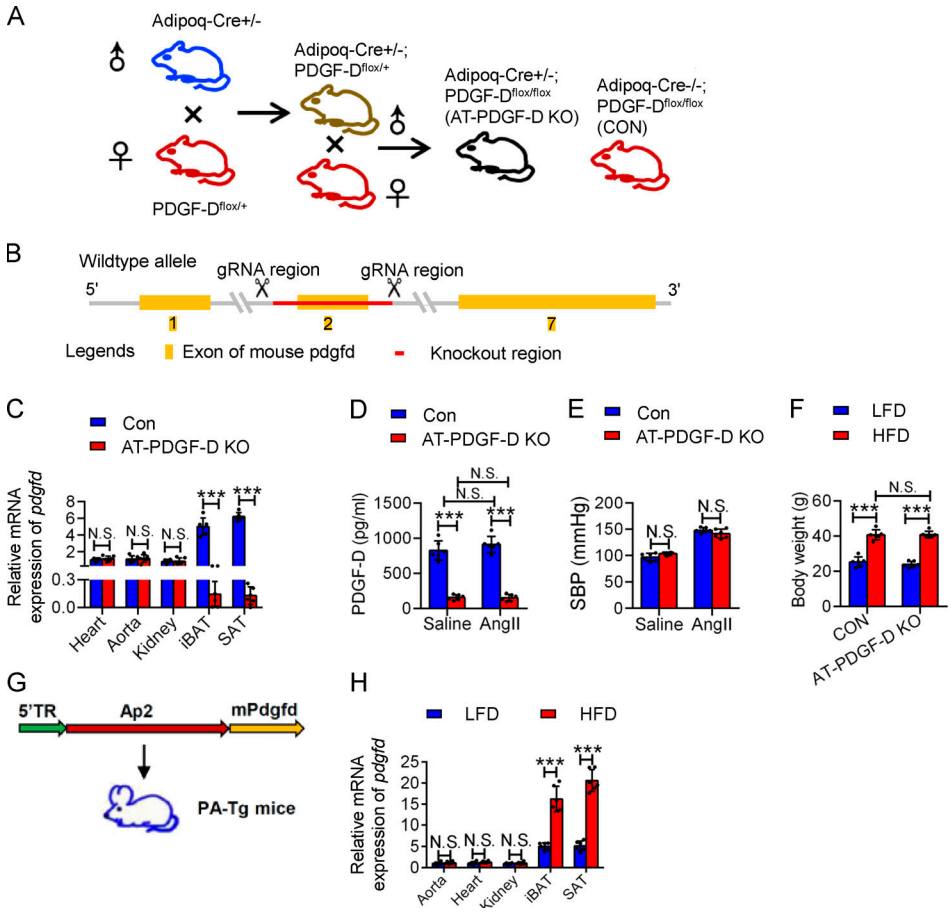

Figure S2. **AT-PDGF-D KO and PA-Tg mice construction. (A)** Diagram of AT-PDGF-D KO construction. **(B)** Construction of global PDGF-D KO mice. Guide (gRNA) was inserted into both sides of exon 2, and then exon 2 was removed by CRISPR/Cas9. **(C)** qPCR analysis of *pdgfd* in heart, aorta, kidney, iBAT, and SAT of Adipoq-Cre−; PDGF-D$^{flox/flox}$ control (Con) and AT-PDGF-D KO obese mice. n = 6. **(D)** PDGF-D level in plasma detected by ELISA. n = 6. **(E)** Systolic blood pressure (SBP) of control and AT-PDGF-D KO obese mice infused with saline or AngII. n = 6. **(F)** Body weight of control and AT-PDGF-D KO mice after 12-wk HFD induction. n = 6. **(G)** Diagram of PA-Tg construction. Adipocyte-specific adipocyte protein 2 (Ap2) promotor was inserted before mouse *pdgfd* gene. **(H)** qPCR analysis of *pdgfd* in heart, aorta, kidney, iBAT, and SAT of WT and PA-Tg mice. n = 6. All experimental data were verified in at least two independent experiments. Statistical significance was assessed using two-way ANOVA with Bonferroni post hoc test. Data are mean ± SD. ***, P < 0.001. TR, translated region.

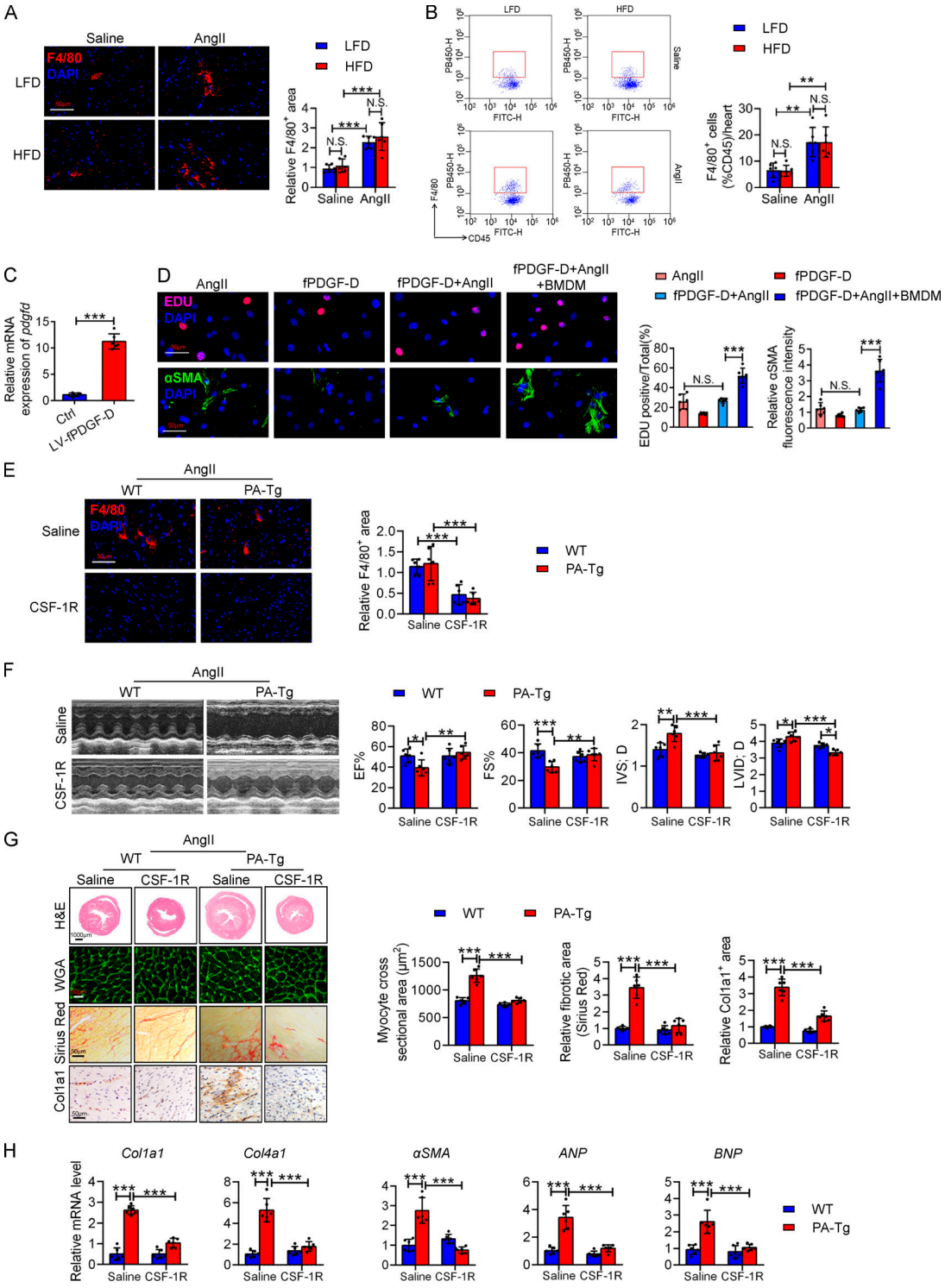

Figure S3. **Macrophages are required in the PDGF-D–aggravated cardiac remodeling in vitro and in vivo. (A and B)** Representative images and quantitative analysis of immunofluorescent staining (A) and flow cytometric analysis (B) of positive macrophage F4/80 in the heart of LFD and HFD mice. *n* = 6. **(C)** qPCR analysis of *pdgfd* in CFs infected with control lentivirus (Ctrl) or full-length PDGF-D shRNA lentivirus (fPDGF-D). *n* = 6. **(D)** Representative images and quantitative analysis of EDU proliferation staining and immunofluorescent staining of αSMA in PDGF-D KO CFs. *n* = 6. **(E)** Representative images and quantitative analysis of immunofluorescent staining of F4/80 in the heart of WT or PA-Tg mice injected with saline or anti-CSF-1R antibody every 2 d during AngII infusion. *n* = 6. **(F)** Representative echocardiography images and quantitative analysis of EF, FS, LVID; D, and IVS; D obtained from echocardiography. *n* = 6. **(G)** Representative cross sections of heart stained for H&E, Sirius Red, and WGA and IHC staining of Col1a1 and quantitative analysis of cardiomyocyte size (WGA staining), fibrotic area (Sirius Red staining), and Col1a1 expression. *n* = 6. **(H)** qPCR analysis of hypertrophic (*ANP* and *BNP*) and fibrotic (*Col1a1*, *Col4a1*, and *αSMA*) genes in the heart. *n* = 6. All experimental data were verified in at least two independent experiments. Statistical significance was assessed using an unpaired two-tailed Student's *t* test (C), one-way ANOVA with Bonferroni post hoc test (D), or two-way ANOVA with Bonferroni post hoc test (A, B, E–H). Data are mean ± SD. *, P < 0.05; **, P < 0.01; ***, P < 0.001. Scale bars, 50 μm except the H&E row in G, which is 1,000 μm.

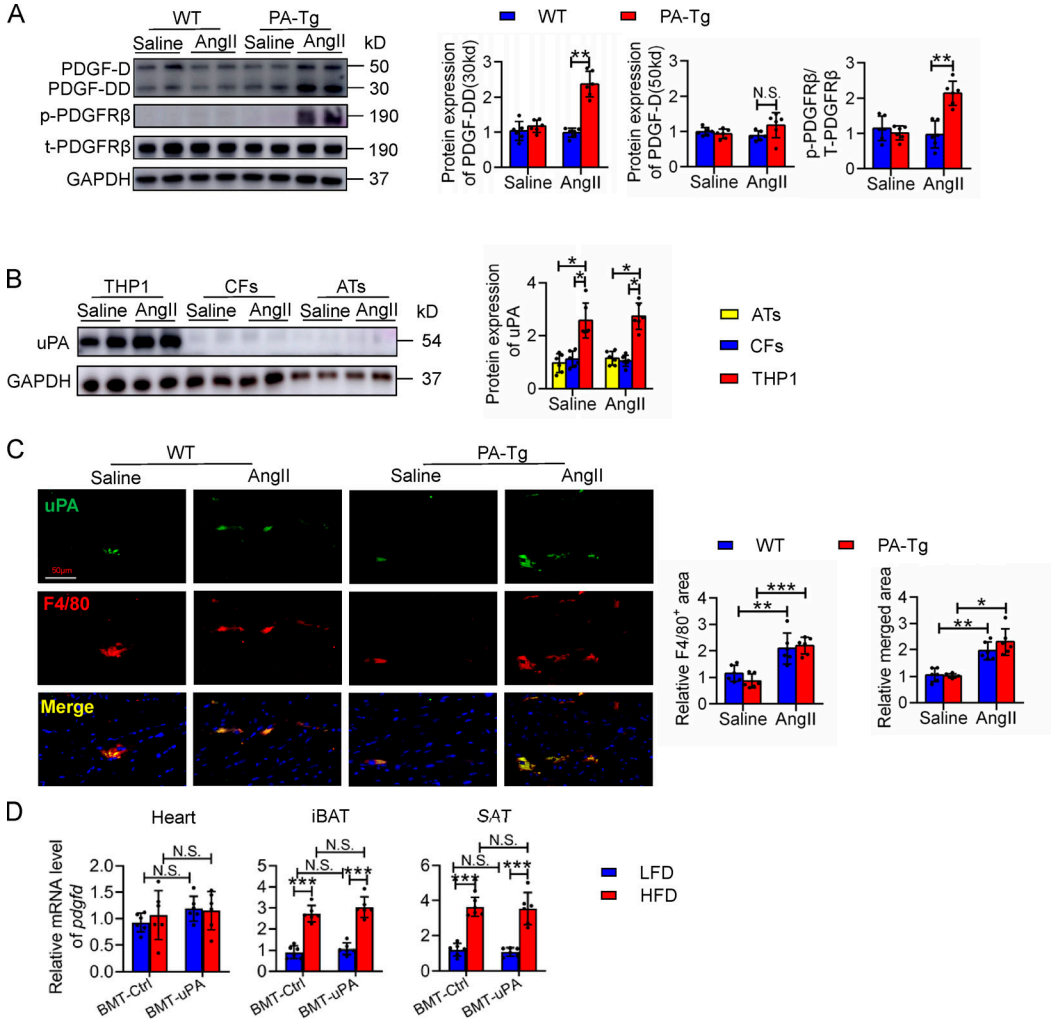

Figure S4. **Macrophage-derived uPA has no effect on PDGF-D expression but activates PDGF-D in hearts of AngII-induced PA-Tg mice. (A)** Western blot and quantitative analysis of PDGF-D, PDGF-DD, p-PDGFRβ, and t-PDGFRβ expression in heart. *n* = 6. **(B)** Western blot and quantitative analysis of uPA expression in CFs, adipocytes (ATs), and differentiated macrophage THP1. *n* = 6. **(C)** Representative images and quantitative analysis of double immunofluorescent staining of uPA and F4/80 in heart of indicated mice. *n* = 6. **(D)** qPCR analysis of *pdgfd* in the heart and adipose tissue of BMT control (Ctrl) and BMT uPA mice. *n* = 6. All experimental data were verified in at least two independent experiments. Statistical significance was assessed using two-way ANOVA with Bonferroni post hoc test. Data are mean ± SD. *, P < 0.05; **, P < 0.01; ***, P < 0.001. Scale bars, 50 μm.

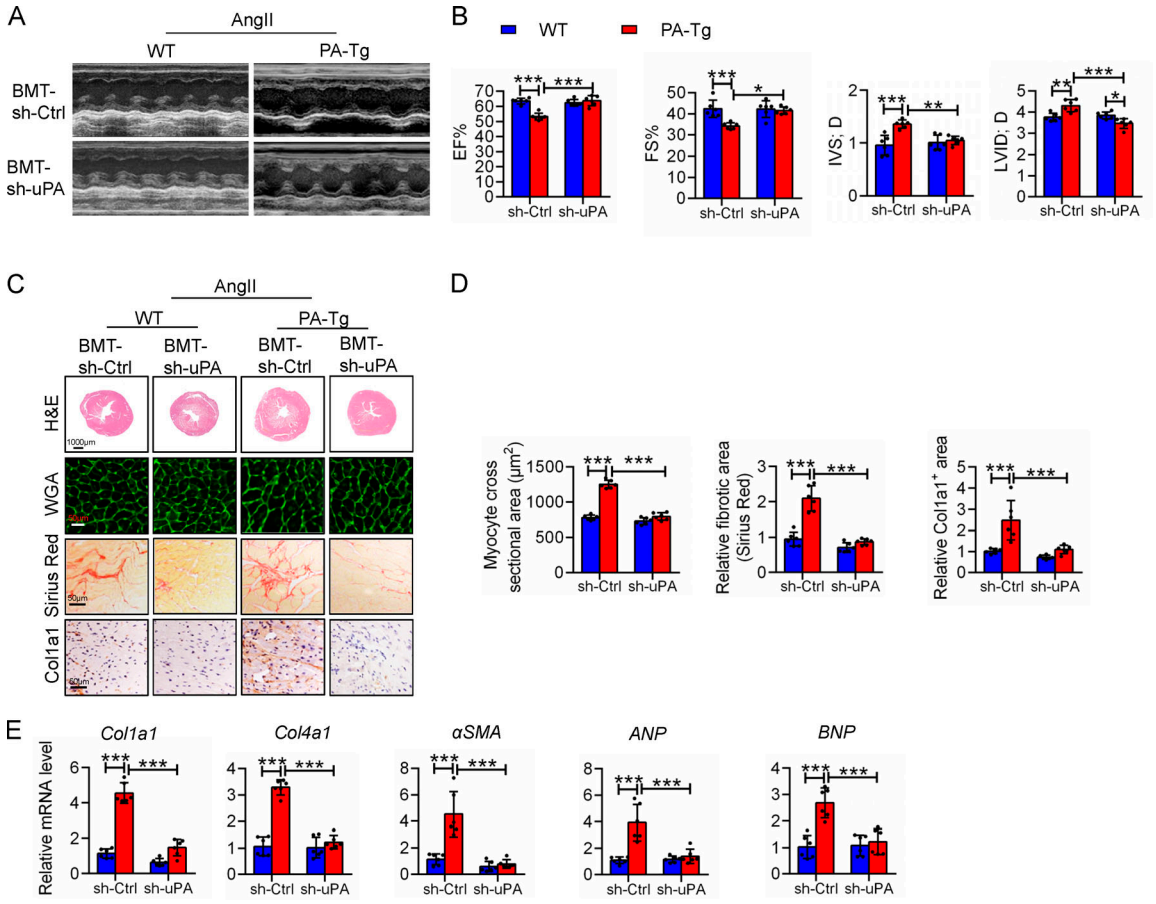

Figure S5. **Macrophage uPA knockdown ameliorates cardiac remodeling of PA-Tg mice. (A)** Representative echocardiography images of AngII-infused WT and PA-Tg mice that received BMT-sh-Ctrl cells or BMT-sh-uPA cells. **(B)** Quantitative analysis of EF, FS, LVID; D, and IVS; D obtained from echocardiography. *n* = 6. **(C)** Representative cross sections of heart stained for H&E, Sirius Red, and WGA and IHC staining of Col1a1. *n* = 6. **(D)** Quantitative analysis of cardiomyocyte size (WGA staining), fibrotic area (Sirius Red staining), and Col1a1 expression. *n* = 6. **(E)** qPCR analysis of hypertrophic (*ANP* and *BNP*) and fibrotic (*Col1a1*, *Col4a1*, and *αSMA*) genes in the heart. *n* = 6. All experimental data were verified in at least two independent experiments. Statistical significance was assessed using two-way ANOVA with Bonferroni post hoc test. Data are mean ± SD. *, P < 0.05; **, P < 0.01; ***, P < 0.001.

Table S1, provided online as a separate Excel file, lists primers for qPCR.